Inorganic Chemistry

pubs.acs.org/IC

Article

Defining the Role of Cr^{3+} as a Reductant in the Hydrothermal Synthesis of $CuCrO_2$ Delafossite

Amanda L. Chown and Byron H. Farnum*

Cite This: https://doi.org/10.1021/acs.inorgchem.2c00943

Read Online

ACCESS | Metrics & More | Article Recommendations | Supporting Information

ABSTRACT: The synthesis of nanocrystalline, p-type delafossite metal oxides ($CuMO_2$) via hydrothermal methods has been explored for a variety of energy conversion and storage applications. However, isolation of the pure phase ternary product is challenging due to the facile growth of unwanted, binary byproducts (CuO, Cu_2O, and M_2O_3) which could ultimately influence the optoelectronic properties of the resulting nanocrystals. Here, we report on the optimized hydrothermal synthesis of $CuCrO_2$ nanocrystals to limit the production of such byproducts. This material possesses a wide band gap and high reported conductivity, making it attractive for applications as the hole transport layer in a variety of heterojunction solar cells. An important aspect of this work is the consideration of Cr^{3+} as the reductant used to reduce Cu^{2+} to Cu^+. This was confirmed by detection and quantification of CrO_4^{2-} as a product of hydrothermal synthesis in addition to the fact that $CuCrO_2$ purity was maximized at a ratio of 4:3 Cr/Cu, consistent with the proposed stoichiometric reaction: $4Cr^{3+} + 3Cu^{2+} + 20\ OH^- \rightarrow 3CuCrO_2 + CrO_4^{2-} + 10\ H_2O$. Using a 4:3 ratio of Cr/Cu starting materials and allowing the synthesis to proceed for 60 h eliminates the presence of CuO beyond detection by powder X-ray diffraction (pXRD). Furthermore, washing the solid product in 0.5 M NH_4OH removes Cu_2O and Cr_2O_3 impurities, leaving behind the isolated $CuCrO_2$ product as confirmed using pXRD and inductively coupled plasma mass spectrometry.

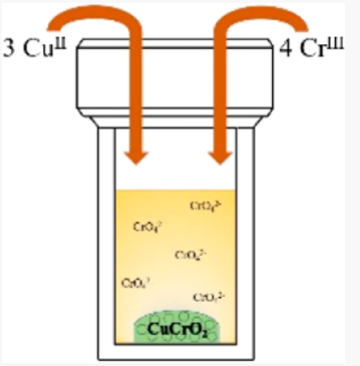

INTRODUCTION

Transparent oxide semiconductors (TOSs), named for both their semiconducting properties and their transparency to visible light due to having a wide band gap, are often used in heterojunction solar cells as charge transport layers. TiO_2, SnO_2, and ZnO are primary examples of n-type TOSs which have been used as electron transport layers in dye-sensitized solar cells, quantum dot solar cells, organic photovoltaics, and perovskite solar cells.[1−6] The examples of p-type TOSs include NiO and the family of $CuMO_2$ delafossites, of which $CuCrO_2$ has been applied as a hole transport layer in various solar cells in addition to solar fuel devices such as dye-sensitized photoelectrosynthesis cells.[7,8]

Previous studies have pointed to the inferior performance for p-type TOSs in comparison to their n-type counterparts, exhibiting short hole diffusion lengths which impede charge extraction.[9,10] It has been proposed that this is due to the electronic defects which result in poor charge separation at the metal oxide interface. Specifically, the proclivity of such defects and byproducts in $CuCrO_2$ synthesis has been linked to the synthetic method, as recently reported by Zhao et al.[11] Understanding these defects thus requires synthetic control of the desired material; however, the synthetic methods used to make delafossite $CuCrO_2$ have been cumbersome. Previous studies required temperatures above 500 °C and high-pressure environments, commonly leading to the phase transition into spinel $CuCr_2O_4$.[12,13] Poeppelmeier developed a hydrothermal synthetic method with Cu_2O and $Cr(OH)_3$ precursors to make $CuCrO_2$ under relatively low temperature conditions, albeit with long reaction times and large particle sizes.[14] In contrast, the hydrothermal synthesis of nanocrystalline delafossite materials is typically achieved with metal salt precursors such as $Cu(NO_3)_2$ and $Cr(NO_3)_3$.[15−17] These routes can be prone to result in cuprite (Cu_2O) and/or tenorite (CuO) side products during the reaction. This has been proposed to result from a gradient in temperature between the walls of the Teflon cup and the solution at the center of the Parr bomb, introducing different thermodynamic environments which may favor byproduct formation.[15]

One aspect of the hydrothermal synthesis from metal salts that has not been addressed is the role of Cr^{3+} as a reductant in the conversion of Cu^{2+} to Cu^+. Although Cu^+ is the desired oxidation state for $CuCrO_2$, Cu^+ is unstable in aqueous solution at room temperature, and thus, Cu^{2+} precursors must be used when starting with metal salts. Ethylene glycol has been used as a reductant for the synthesis of $CuGaO_2$ where Ga^{3+} is redox inert. Likewise, the synthesis of $CuFeO_2$ has been achieved with either ethylene glycol or Fe^{2+} as the reductant.

Received: March 22, 2022

Despite the obvious need for a reductant, published synthetic procedures for $CuCrO_2$ from metal salt precursors have not included a secondary reductant or discussed the redox activity of Cr^{3+} such that no stoichiometric reaction has been established for the overall synthesis. Given the challenges of competitive binary oxide formation present in the ternary $CuCrO_2$ synthesis in addition to the possible consumption of Cr^{3+} due to redox activity, understanding the optimized stoichiometry for Cr/Cu is an important parameter for achieving pure phase $CuCrO_2$.

Here, we report on the hydrothermal synthesis and optimization of $CuCrO_2$ in an effort to produce nanocrystalline materials in the absence of unwanted byproducts. By optimizing the synthetic conditions for the growth of $CuCrO_2$, photo/electrochemical studies may be more reproducible and the material may be better understood fundamentally for further applications. Here, we show that the ratio of starting materials, in addition to the production of chromate, clearly has an influence on byproduct formation, where a 4:3 ratio of Cr^{3+} and Cu^{2+} nitrate salts is optimal for hydrothermal synthesis of $CuCrO_2$.

EXPERIMENTAL SECTION

Synthesis of $CuCrO_2$ Nanocrystals. Hydrothermal synthesis of delafossite $CuCrO_2$ nanocrystals was conducted according to a preparation method previously reported in the literature.[14,18] Chromium nitrate nonahydrate $[Cr(NO_3)_3{\cdot}9H_2O]$ (Alfa Aesar, 98.5%) and copper nitrate hemipentahydrate $[Cu(NO_3)_2{\cdot}2.5H_2O]$ (Alfa Aesar, 98%+) were added to 70 mL of deionized H_2O (18MΩ cm, Milli-Q) and stirred in an ice bath. The molar ratio of chromium to copper precursors (Cr/Cu) was varied to generate two series of reaction conditions. Series 1 contained Cr/Cu ratios from 0.5 to 10 in which the total metal concentration was held constant at [Cr] + [Cu] = 0.5 M. Series 2 contained Cr/Cu ratios from 0.5 to 2 in which [Cu] = 0.21 M was fixed. After the addition of precursors to cold water, a minimum of 7.03 g of KOH (VWR Analytical) was added, and a final targeted pH > 13 was recorded to ensure the basicity of the solution and visual confirmation of metal hydroxide formation in solution.

The mixture was then stirred and transferred equally to three 45 mL Teflon cups and sealed in acid digestion bombs (Parr). The bombs were placed in a box furnace (Lindberg Blue M) and heated to 240 °C for 12−60 h, depending on the procedure. The bombs were removed from the furnace and the reaction mixtures were centrifuged to separate the solid products, which were combined to form a single solid product. This solid was analyzed for structural characterization prior to being suspended in 0.5 M NH_4OH (28 vol %, BDH) solution for 24 h. Following this step, any dissolved solid was rinsed with ethanol, sonicated in ethanol, and vortexed for three cycles to remove impurities and to clean the product. The remaining product was allowed to dry in ethanol under a fume hood before the final drying step in a vacuum oven (Lindberg Blue M) at 60 °C.

Analysis of CrO_4^{2-}. In order to study the role of Cr^{3+} as a reducing agent, the chromate produced from each reaction was quantified spectrophotometrically. Standard, tech-grade $Na_2Cr_2O_7$ was added to a basic solution with a pH ≥ 13 containing KOH in Millipore H_2O to prepare standard chromate solutions at known concentrations. At pH 13, $Cr_2O_7^{2-}$ dissociates completely to form two equivalents of CrO_4^{2-}.[19] The extinction coefficient of the absorbance peak for CrO_4^{2-} at 372 nm was then quantified using UV−visible absorbance spectroscopy. The pH of post-synthesis solutions was found to be in excess of 13, ensuring CrO_4^{2-} quantification. An Agilent Cary 8454 UV−vis spectrophotometer was used to study both the standard and experimental concentrations of chromate ions in solution.

Structural Characterization. Powder X-ray diffraction (pXRD) data was collected using a Rigaku SmartLab X-ray diffractometer with a Cu Kα source in a Bragg−Brentano geometry. The XRD data were processed using SmartLab Studio II software. Scanning electron microscopy (SEM) images were collected using a Hitachi S-4700. Transmission electron microscopy (TEM) images were collected using a Thermo Scientific Talos F200X with EDS. Inductively coupled plasma mass spectrometry (ICP-MS) was collected using an Agilent 7900 Quadrupole ICP-MS system with a high-temperature (>6000 K) plasma source. All samples were dissolved in trace metal-free concentrated nitric acid by means of hydrothermal acid digestion in Teflon Parr bombs at 200 °C for 5 h. A serial dilution was performed using a trace metal-free 2% nitric acid solution to acquire an ICP-ready solution with a targeted sample concentration between 0 and 200 ppb.

RESULTS AND DISCUSSION

A 1:1 ratio of Cr/Cu starting material has been commonly used in the literature to produce delafossite $CuCrO_2$. However, the time required to undergo the condensation reaction of the precursors, as can be seen in Figure 1, is unclear. While some

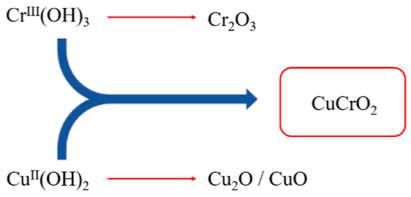

Figure 1. Illustration of the general condensation reaction producing the delafossite metal oxide $CuCrO_2$ with competitive formation of binary oxides Cu_2O, CuO, and Cr_2O_3.

reported 60 h reactions previously,[14,20] others have reported producing $CuCrO_2$ under shorter reaction times.[11,21] Before further synthetic optimization, we explored the time dependence of the reaction using the hydrothermal synthetic route to determine if allowing the synthesis to proceed for a longer period of time improves the overall quality of the product.

As can be seen in Figure 2, a series of reactions were conducted where the ratio of the Cr/Cu starting materials was

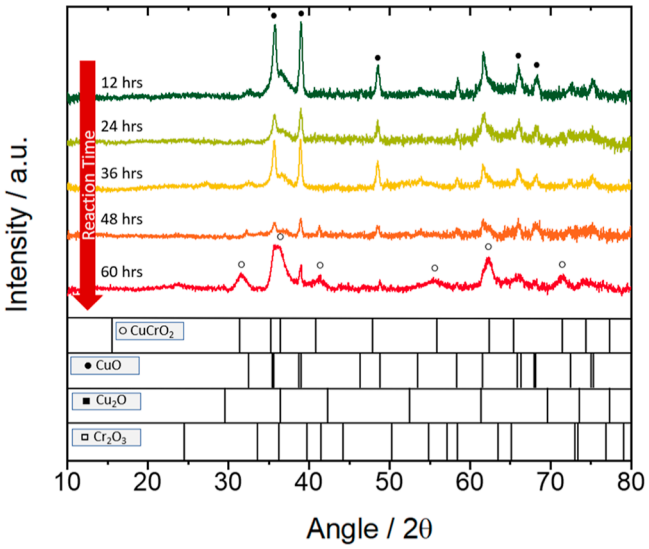

Figure 2. pXRD diffractograms obtained from unwashed solid products resulting from a 1:1 Cr/Cu ratio with various reaction times from 12 to 60 h. Standard diffraction patterns for CuO (PDF 00-041-0254), Cu_2O (PDF 00-005-0667), Cr_2O_3 (PDF 00-038-1479), and $CuCrO_2$ (PDF 00-039-0247) are shown for comparison.

https://doi.org/10.1021/acs.inorgchem.2c00943
Inorg. Chem. XXXX, XXX, XXX−XXX

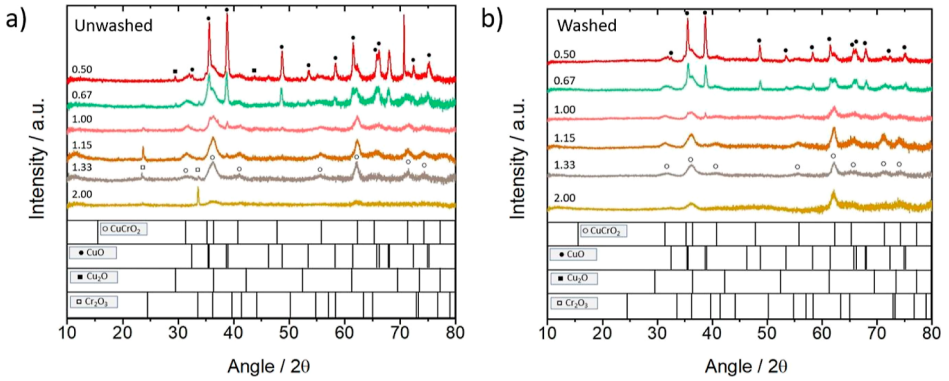

Figure 3. Powder diffractograms obtained for solid products for the indicated Cr/Cu ratios with a reaction time of 60 h. In all cases, [Cr] + [Cu] = 0.5 M. Peaks from $CuCrO_2$ are identified using (○) and peaks from CuO are identified using (●). Noteworthy peaks from Cu_2O and Cr_2O_3 are denoted using (■) and (□), respectively. (a) Unwashed samples. (b) Samples after being washed in 0.5 M NH_4OH solution for 24 h.

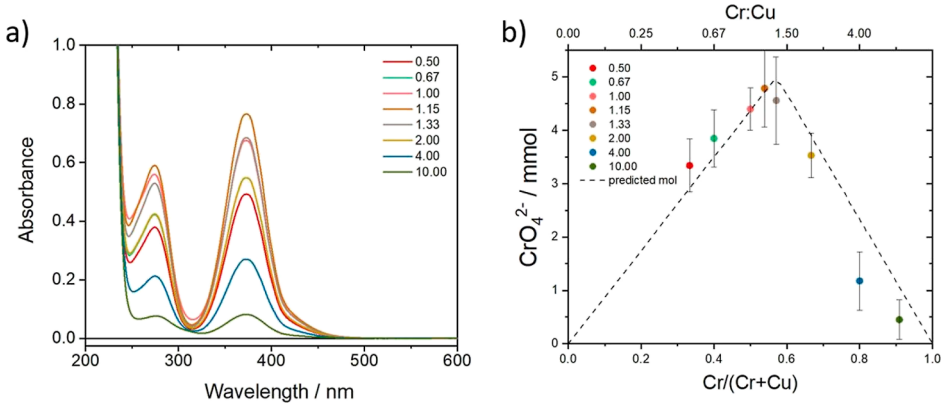

Figure 4. a) UV−visible absorbance spectra of post-reaction solutions produced from different ratios of Cr/Cu with a total [Cr] + [Cu] = 0.5 M. The absorbance spectra are consistent with CrO_4^{2-}. (b) Millimoles of CrO_4^{2-} measured from absorbance data plotted vs mole fraction of Cr and Cr/Cu ratio. The dashed line shows the theoretical amount of CrO_4^{2-} produced based on eq 1.

fixed at 1:1 with 0.5 M total starting materials (i.e., 0.25 M each), and the reaction time was varied from 12, 24, 36, 48, and 60 h. Under the 12 h synthesis condition, it is apparent that three distinct peaks at 35.5, 38.8, and 48.8° are present. These peaks are specific to the diffraction pattern for CuO (tenorite; PDF #00-041-0254). A broad shoulder peak near 37° was also evident and could be assigned to either Cu_2O or $CuCrO_2$. Diffractograms were found to be unchanged from 12 to 48 h; however, as the reaction time increased to 60 h, the peaks associated with CuO decreased in intensity, and the predominant peaks in the diffractogram were found to be 31.0, 36.2, and 61.7°, characteristic of the (006), (012), and (110) peaks, respectively, for delafossite $CuCrO_2$ (PDF #00-039-0247). Notably, even at 60 h, residual peaks for CuO were still observed at 38.8 and 48.8°. This could suggest that CuO is a precursor to $CuCrO_2$ formation or that Cu^{2+} is insufficiently reduced to Cu^+. Based on these results, the synthetic time was fixed at 60 h for all subsequent experiments to allow for optimal formation of $CuCrO_2$.

To investigate the role of Cr^{3+} as a reductant, metal oxide powders were synthesized using a constant total concentration of metal [Cr] + [Cu] = 0.5 M while the moles of $Cu(NO_3)_2$ and $Cr(NO_3)_3$ were adjusted in order to vary the ratio of Cr/Cu from 0.50 to 2.00. The XRD data for the unwashed solids are shown in Figure 3a. Reaction parameters for the series can be found in Table S1 for additional clarity. Control experiments with only 0.5 M $Cu(NO_3)_2$ or $Cr(NO_3)_3$ are also shown for reference in Figure S1. Clear changes in the diffractograms were observed as a function of Cr/Cu ratio with Cr/Cu = 0.50 and 0.67 showing sharp, pronounced peaks for CuO (35.5, 38.8, and 48.8°) and much smaller, broad peaks for $CuCrO_2$ (31.0, 36.2, and 61.7°). The broad peaks of $CuCrO_2$ indicate nanocrystalline particle sizes. Under the condition where only $Cu(NO_3)_2$ was present (Cr/Cu = 0.00), CuO was the only observed product. When looking at Cr/Cu = 1.00, 1.15, and 1.33 diffractograms, it is evident that the broad peaks assigned to $CuCrO_2$ became dominant while those for CuO were greatly diminished, being undetectable for Cr/Cu = 1.33. At the highest Cr/Cu = 2.00, CuO could not be detected by pXRD.

To determine the limit of detection of CuO, pXRD data was collected for varying mixtures of NaCl and CuO standards, as can be seen in Figure S2. It is evident that even at 1 wt % CuO, peaks identified as CuO were present in the powder mixtures. Therefore, an absence of CuO peaks can be assigned to <1% impurity.

Additionally, peaks associated with Cu_2O and Cr_2O_3 are present in Figure 2a. Washing the solid product with 0.5 M NH_4OH for 24 h resulted in the removal of peaks assigned to Cu_2O and Cr_2O_3; however, CuO peaks were persistent (Figure 3b). These results show that $CuCrO_2$ of high purity could be synthesized using a Cr/Cu ratio greater than 1.33 coupled with a secondary washing step in NH_4OH. These results also

https://doi.org/10.1021/acs.inorgchem.2c00943
Inorg. Chem. XXXX, XXX, XXX−XXX

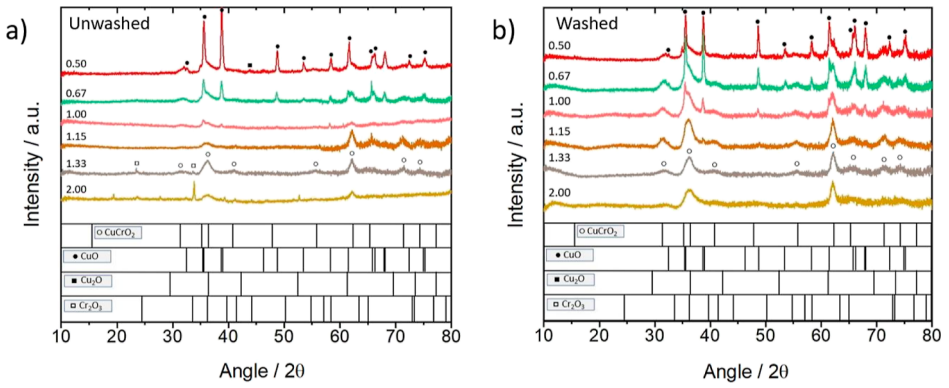

Figure 5. Powder diffractograms obtained for solid products from the indicated Cr/Cu ratios. In all cases, the total $[Cu^{2+}]$ = 0.21 M (i.e., 15 mmol). Peaks from $CuCrO_2$ are identified using (○) and peaks from CuO are identified using (●). Noteworthy peaks from Cu_2O and Cr_2O_3 are denoted using (□) and (■). (a) Unwashed solids. (b) Solids after being washed in 0.5 M NH_4OH solution for 24 h.

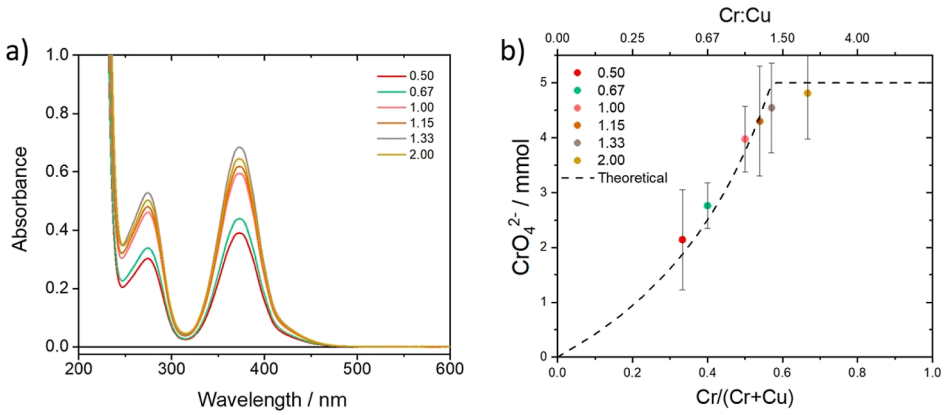

Figure 6. a) UV−visible absorbance spectra of post-reaction solutions produced from reactions where [Cu] = 0.21 M. (b) Millimoles of CrO_4^{2-} in solution for each reaction calculated from absorbance data and plotted vs mole fraction of Cr and Cr/Cu ratio. The dashed line represents the theoretical amount of CrO_4^{2-} based on eq 1.

suggest that many literature procedures which utilize a 1:1 Cr/Cu ratio may have CuO impurities.

The product formation as a function of Cr/Cu ratio strongly suggests that Cr^{3+} acts as a reductant for conversion of Cu^{2+} to Cu^{+}. In the absence of Cr^{3+} or with a Cr/Cu ratio <1.00, CuO was predominately formed, whereas with higher ratios, the Cu^{+}-containing $CuCrO_2$ was the dominant product. A proposed redox reaction for the overall formation of $CuCrO_2$ is shown in eq 1, where one Cr^{3+} is able to reduce three equivalents of Cu^{2+} to Cu^{+}, resulting in a balanced stoichiometry of 4:3 Cr/Cu (1.33). In further support of this, calculated Pourbaix diagrams reported by Beverskog show that reduction of Cu^{2+} by Cr^{3+} is thermodynamically favorable at elevated temperatures with $\Delta G = -0.33$ eV at 200 °C (see the Supporting Information for further details).[22,23] Equation 1 was confirmed by the presence of CrO_4^{2-} as the oxidized product, as determined by UV−visible absorbance spectra collected for the post-synthesis reaction liquid (Figure 4a). The concentration of CrO_4^{2-} produced for each Cr/Cu ratio was then calculated using the extinction coefficient of the absorbance feature at 372 nm, measured to be 4835 M^{-1} cm^{-1} (Figure S3) and consistent with other literature reports.[24−26]

$$4Cr^{3+} + 3Cu^{2+} + 20OH^- \rightarrow 3CuCrO_2 + CrO_4^{2-} + 10H_2O \quad (1)$$

$$2Cr^{3+} + 6Cu^{2+} + 22OH^- \rightarrow 3Cu_2O + 2CrO_4^{2-} + 11H_2O \quad (2)$$

Figure 4b shows the concentration of chromate ions produced as a function of mole fraction of Cr (χ_{Cr} = Cr/(Cr + Cu)) and Cr/Cu ratio. It is evident that the largest amount of chromate produced is near the optimal ratio of 1.33 for Cr/Cu reactants (χ_{Cr} = 0.57). Error bars are provided and represent the standard deviation calculated from three separate reactions. The increase in CrO_4^{2-} up to 1.33 Cr/Cu followed by a decrease at higher ratios is due to the constant total metal concentration used for this series of reactions. At low Cr/Cu ratios, the amount of CrO_4^{2-} produced is limited by the amount of Cr^{3+} present during the reaction and the efficiency of reduction. At high Cr/Cu ratios, CrO_4^{2-} production is limited by the amount of Cu^{2+} available. The dashed line shown in Figure 4b represents the theoretical amount of CrO_4^{2-} produced for 100% efficiency of eq 1.

The experimental data follows the expected trend with additional data points at Cr/Cu ratios of 4.00 and 10.00 continuing to show the linear decline in CrO_4^{2-} with Cr/Cu and χ_{Cr}; however, the experimental data deviates from the theoretical line at ratios both lower and higher than 1.33. These deviations are a reflection of the percent yield for CrO_4^{2-} (Table S3) and were found to be greater than that expected for Cr/Cu < 1.33 and lower than that expected for Cr/Cu > 1.33. For Cr/Cu < 1.33, we believe that competitive

https://doi.org/10.1021/acs.inorgchem.2c00943
Inorg. Chem. XXXX, XXX, XXX−XXX

formation of Cu_2O via reduction of Cu^{2+} by Cr^{3+} is responsible for the greater than 100% yield of CrO_4^{2-}. The balanced redox reaction for the Cu_2O formation is shown in eq 2 where the yield of CrO_4^{2-} per Cr^{3+} is 100% compared with 25% for $CuCrO_2$ formation. A small fraction of Cu_2O side reactivity could therefore produce a greater than expected yield for CrO_4^{2-}. For Cr/Cu > 1.33, we believe that the decline in percent yield is due to competitive Cr_2O_3 formation as more Cr^{3+} is introduced to the reaction. In addition, the decreased percent yields at higher Cr/Cu ratios indicates a lower efficiency for Cr^{3+} reduction of Cu^{2+}, which is supported by the persistent nature of CuO found via pXRD at higher ratios.

To further confirm the Cr^{3+}-reductant mechanism, a second series of reactions was conducted where the ratio of Cr/Cu was varied from 0.50 to 2.00; however, the $Cu(NO_3)_2$ starting material was fixed at 0.21 M (i.e., 15 mmol), allowing both the amount of $Cr(NO_3)_3$ and the amount of total metal concentration to change. Reaction parameters for the series can be found in Table S2. The pXRD data showed similar trends as the first series, with high amounts of CuO at low Cr/Cu ratios, optimal production of $CuCrO_2$ at 1.33 Cr/Cu, and an increase in Cr_2O_3 at high Cr/Cu ratios (Figure 5).

The amount of CrO_4^{2-} produced experimentally for the second series followed the predicted theoretical trend (Figure 6) where production was limited at low Cr/Cu ratios by the amount of Cr^{3+} in solution and reached a plateau beyond a ratio of 1.33 due to the constant amount of Cu^{2+}. Notably, reactions containing Cr/Cu ratios of 4.00 and 10.00 were not conducted with this series because the amount of Cr^{3+} reactant needed to run the reaction became impractical beyond a 2.00 ratio. Similar to the first series, the percent yield was also found to be greater than 100% at low Cr/Cu ratios and decrease as the ratio increased. Figure S4 shows an overlay of CrO_4^{2-} percent yields for both series of reactions where both show a similar decline as Cr/Cu increased. Also consistent was the fact that low Cr/Cu ratios resulted in CrO_4^{2-} percent yields in excess of 100%, likely due to Cu_2O formation according to eq 2.

Microscopy studies were conducted on samples from each series to analyze the morphological characteristics of each product. The SEM images collected for series 1 reactions after base washing are shown in Figure 7. Figure S5 shows the SEM data for series 2 reactions. Across all reaction conditions, small particles were produced with anisotropic, plate-like morphology appearing for ratios of 1.00 and 1.33. The plate-like morphology is characteristic of $CuCrO_2$ nanocrystals based on the layered delafossite unit cell. At Cr/Cu = 0.50, more isotropic particles with smooth faces are observed. This could be due to the CuO formation under conditions where an excess amount of Cu^{2+} starting material was used. Indeed, when only Cu^{2+} was present in the reaction, the CuO produced exhibited an isotropic morphology, albeit with large particle sizes (Figure S6). In the reaction with only Cr^{3+}, small amorphous particles were produced.

TEM and EDS studies were further conducted on the optimized Cr/Cu ratio of 1.33 with images shown in Figure 8. Nanocrystals appear as anisotropic plates with an aspect ratio of 3.4 ± 0.5. High magnification indicates lattice fringes labeled A and B in Figure 8c, typical of other reports for TEM images of $CuCrO_2$ nanocrystals.[27,28] High-angle annular dark-field images and EDS mapping reveal an even distribution of copper, chromium, and oxygen atoms throughout the nanocrystals.

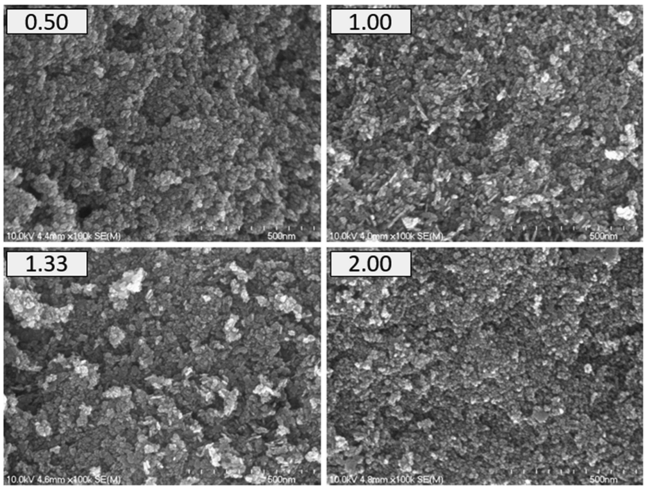

Figure 7. SEM images at constant magnification of products with Cr/Cu ratios 0.50, 1.00, 1.33, and 2.00 from the series with [Cr] + [Cu] = 0.5 M. All samples have been washed in 0.1 M NH_4OH solution for 24 h.

ICP-MS was conducted for each sample in both series to determine the elemental composition. A summary of this data is shown in Table 1 for the unwashed and base-washed products. The measured Cr/Cu ratio for unwashed samples was found to be an average of 73 ± 7% of the starting ratio across all reaction conditions, indicating that ∼27% of the starting precursors do not get converted to the solid product. The low ratios for the solid product obtained from low starting ratios is consistent with the presence of CuO byproducts found via pXRD, resulting from a lack of Cu^{2+} reduction at low concentrations of Cr^{3+}. As Cr/Cu increased beyond the optimal ratio of 1.33, the final ratio also increased, likely due to the formation of Cr_2O_3 byproducts or other amorphous materials not detectable by XRD in excess of $CuCrO_2$. Washing the solid products resulted in a general increase in the final Cr/Cu ratio, likely due to removal of Cu_2O.

Based on the pXRD and ICP analysis, the optimal ratio of Cr/Cu to form $CuCrO_2$ with minimal impurities is 1.33 (4:3). At this ratio, an excess of Cu is present in the unwashed sample, which is likely attributed to the presence of Cu_2O impurity. After base washing the product, the ratio increased due to removal of Cu_2O (i.e., 27% mass loss during the washing step; Table S4) and resulted in a final Cr/Cu ratio of 1.04, indicating a slight excess of Cr. Based on pXRD, this solid product is expected to be free from CuO impurities, and thus, the excess Cr could be attributed to Cu^+ vacancies in the $CuCrO_2$ lattice. This means that ∼4% of Cu^+ sites could be vacant. Previous studies on $CuGaO_2$ have also indicated Cu^+ vacancies at similar defect percentages.[29]

The role of Cr^{3+} as a reductant is clearly established by the data presented thus far; however, the complexities of the competitive reactions beg the question of whether an alternative reductant could be used to generate Cu^+ while keeping the Cr^{3+} redox stable. The other reported synthetic routes for copper delafossite materials have used ethylene glycol as a reductant with much success.[30−32] For comparative purposes, ethylene glycol was thus added to the reaction with a 1:1 ratio of Cr/Cu precursors, as an excess of Cr should not be needed. Analysis of the solid product by pXRD (Figure 9), however, revealed that $CuCrO_2$ was not formed, but rather Cu metal (PDF #00-004-0836) was the major product along with

https://doi.org/10.1021/acs.inorgchem.2c00943
Inorg. Chem. XXXX, XXX, XXX−XXX

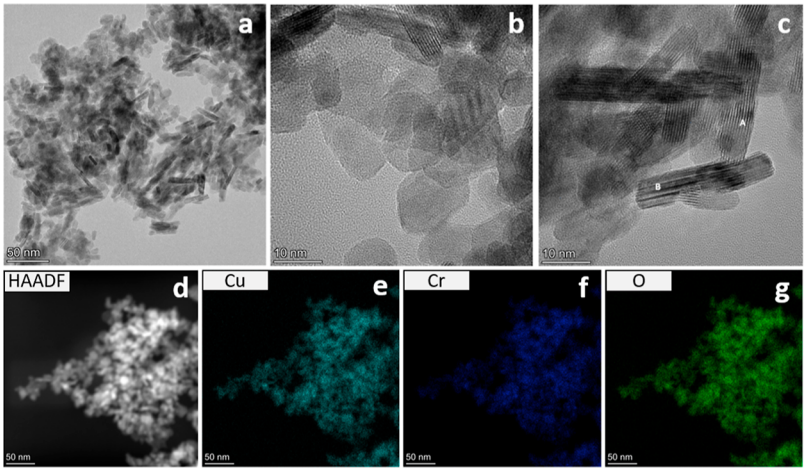

Figure 8. (a–c) TEM images of the washed solid product obtained from a Cr/Cu ratio of 1.33 with [Cu] + [Cr] = 0.5 M. (d–g) HAADF images and EDS mapping of the same material.

Table 1. Ratio of Cr/Cu Measured by ICP-MS for Solid Products

	[Cu] + [Cr] = 0.5 M		[Cu] = 0.21 M	
starting ratio	unwashed	washed	unwashed	washed
0.50	0.365 ± 0.004	0.402 ± 0.005	0.311 ± 0.004	0.325 ± 0.003
0.67	0.505 ± 0.006	0.511 ± 0.014	0.579 ± 0.008	0.547 ± 0.009
1.00	0.647 ± 0.006	0.766 ± 0.014	0.743 ± 0.027	0.753 ± 0.009
1.15	0.885 ± 0.022	0.889 ± 0.014	0.749 ± 0.012	0.843 ± 0.016
1.33	0.940 ± 0.059	1.036 ± 0.015	0.940 ± 0.059	1.036 ± 0.015
2.00	1.523 ± 0.006	1.685 ± 0.033	1.625 ± 0.019	1.680 ± 0.033

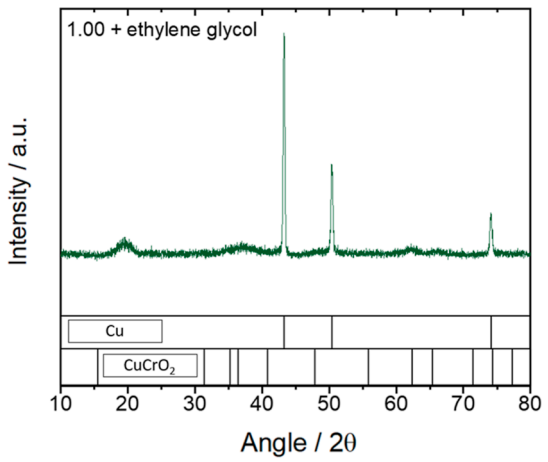

Figure 9. Diffractogram for the solid product obtained from hydrothermal synthesis of a 1:1 ratio of Cr/Cu for 60 h with ethylene glycol added as a reductant.

an unknown product, possibly derived from Cr. These results indicate that addition of secondary reductants is not likely to result in a more efficient synthesis of $CuCrO_2$ and that a solid understanding of the Cr^{3+} reductant and competitive side reactions is required to produce $CuCrO_2$ nanocrystals of high purity.

CONCLUSIONS

The role of Cr^{3+} as a reductant in the hydrothermal synthesis of $CuCrO_2$ from Cu^{2+} and Cr^{3+} precursors has been clearly elucidated by detection of CrO_4^{2-} in the post-synthesis reaction solution. The results point to an optimized Cr/Cu ratio of 4:3 based on the reaction stoichiometry established in eq 1. Deviation from this ratio leads to the formation of byproducts such as Cu_2O, CuO, and Cr_2O_3. The narrow window for which $CuCrO_2$ can be synthesized with high purity emphasizes the fact that impurities and defects could influence the optical or electrochemical properties of $CuCrO_2$ if synthetic parameters are not optimized. Future studies are currently underway to understand how these impurities and defects specifically impact the electrochemical properties and the band gap of $CuCrO_2$.

ASSOCIATED CONTENT

Supporting Information

The Supporting Information is available free of charge at https://pubs.acs.org/doi/10.1021/acs.inorgchem.2c00943.

XRD, UV–visible absorbance, SEM, mass yields, and redox chemistry (PDF)

AUTHOR INFORMATION

Corresponding Author

Byron H. Farnum − *Department of Chemistry and Biochemistry, Auburn University, Auburn, Alabama 36849, United States;* orcid.org/0000-0001-9152-1909; Email: farnum@auburn.edu

Author

Amanda L. Chown − *Department of Chemistry and Biochemistry, Auburn University, Auburn, Alabama 36849, United States*

Complete contact information is available at: https://pubs.acs.org/10.1021/acs.inorgchem.2c00943

https://doi.org/10.1021/acs.inorgchem.2c00943
Inorg. Chem. XXXX, XXX, XXX−XXX

Notes

The authors declare no competing financial interest.

■ ACKNOWLEDGMENTS

The authors thank Auburn University for supporting this research. pXRD data collection was performed using a Rigaku SmartLab diffractometer purchased through support from the National Science Foundation Major Research Instrumentation program under award number NSF-DMR-2018794. The authors also thank Prof. David Stanbury for helpful discussions, Dr. Amar Kumbhar for SEM and TEM data collection at the CHANL facility located at the University of North Carolina at Chapel Hill, and Dr. Mehmet Zeki Billor for ICP-MS data collection at the Auburn University Department of Geosciences ICP-MS Lab facility.

■ REFERENCES

(1) Samadpour, M.; Boix, P. P.; Giménez, S.; Zad, A. I.; Taghavinia, N.; Mora-Seró, I.; Bisquert, J. Fluorine Treatment of TiO2 for Enhancing Quantum Dot Sensitized Solar Cell Performance. *J. Phys. Chem. C* **2011**, *115*, 14400−14407.

(2) Boix, P. P.; Larramona, G.; Jacob, A.; Delatouche, B.; Mora-Seró, I.; Bisquert, J. Hole Transport and Recombination in All-Solid Sb2S3-Sensitized TiO2 Solar Cells Using CuSCN As Hole Transporter. *J. Phys. Chem. C* **2012**, *116*, 1579−1587.

(3) Dembele, K. T.; Selopal, G. S.; Soldano, C.; Nechache, R.; Rimada, J. C.; Concina, I.; Sberveglieri, G.; Rosei, F.; Vomiero, A. Hybrid Carbon Nanotubes−TiO2 Photoanodes for High Efficiency Dye-Sensitized Solar Cells. *J. Phys. Chem. C* **2013**, *117*, 14510−14517.

(4) Yang, K.; Fu, J.; Hu, L.; Xiong, Z.; Li, M.; Wei, X.; Xiao, Z.; Lu, S.; Sun, K. Impact of ZnO Photoluminescence on Organic Photovoltaic Performance. *ACS Appl. Mater. Interfaces* **2018**, *10*, 39962−39969.

(5) Xu, Z.; Jiang, Y.; Li, Z.; Chen, C.; Kong, X.; Chen, Y.; Zhou, G.; Liu, J.-M.; Kempa, K.; Gao, J. Rapid Microwave-Assisted Synthesis of SnO2 Quantum Dots for Efficient Planar Perovskite Solar Cells. *ACS Appl. Energy Mater.* **2021**, *4*, 1887−1893.

(6) Rao, A. D.; Karalatti, S.; Thomas, T.; Ramamurthy, P. C. Self-Assembled, Aligned ZnO Nanorod Buffer Layers for High-Current-Density, Inverted Organic Photovoltaics. *ACS Appl. Mater. Interfaces* **2014**, *6*, 16792−16799.

(7) Dimple, D.; Lebègue, S.; Pastore, M. Dye Anchoring on CuCrO2 Surfaces for P-Type Dye-Sensitized Solar Cell Applications: An Ab Initio Study. *ACS Appl. Energy Mater.* **2021**, *4*, 6180−6190.

(8) Powar, S.; Xiong, D.; Daeneke, T.; Ma, M. T.; Gupta, A.; Lee, G.; Makuta, S.; Tachibana, Y.; Chen, W.; Spiccia, L.; Cheng, Y.-B.; Götz, G.; Bäuerle, P.; Bach, U. Improved Photovoltages for P-Type Dye-Sensitized Solar Cells Using CuCrO2 Nanoparticles. *J. Phys. Chem. C* **2014**, *118*, 16375−16379.

(9) Kawazoe, H.; Yasukawa, M.; Hyodo, H.; Kurita, M.; Yanagi, H.; Hosono, H. P-Type Electrical Conduction in Transparent Thin Films of CuAlO2. *Nature* **1997**, *389*, 939−942.

(10) Hautier, G.; Miglio, A.; Ceder, G.; Rignanese, G.-M.; Gonze, X. Identification and Design Principles of Low Hole Effective Mass P-Type Transparent Conducting Oxides. *Nat. Commun.* **2013**, *4*, 2292.

(11) Zhao, R.-D.; Zhang, Y.-M.; Liu, Q.-L.; Zhao, Z.-Y. Effects of the Preparation Process on the Photocatalytic Performance of Delafossite CuCrO2. *Inorg. Chem.* **2020**, *59*, 16679−16689.

(12) Shannon, R. D.; Rogers, D. B.; Prewitt, C. T. Chemistry of Noble Metal Oxides. I. Syntheses and Properties of ABO2 Delafossite Compounds. *Inorg. Chem.* **1971**, *10*, 713−718.

(13) Croft, W. J.; Tombs, N. C.; England, R. E. Crystallographic Data for Pure Crystalline Silver Ferrite. *Acta Crystallogr.* **1964**, *17*, 313.

(14) Sheets, W. C.; Mugnier, E.; Barnabé, A.; Marks, T. J.; Poeppelmeier, K. R. Hydrothermal Synthesis of Delafossite-Type Oxides. *Chem. Mater.* **2006**, *18*, 7−20.

(15) Wang, J.; Ibarra, V.; Barrera, D.; Xu, L.; Lee, Y.-J.; Hsu, J. W. P. Solution Synthesized P-Type Copper Gallium Oxide Nanoplates as Hole Transport Layer for Organic Photovoltaic Devices. *J. Phys. Chem. Lett.* **2015**, *6*, 1071−1075.

(16) Kumar, S.; Miclau, M.; Martin, C. Hydrothermal Synthesis of AgCrO2 Delafossite in Supercritical Water: A New Single-Step Process. *Chem. Mater.* **2013**, *25*, 2083−2088.

(17) Xiong, D.; Zeng, X.; Zhang, W.; Wang, H.; Zhao, X.; Chen, W.; Cheng, Y.-B. Synthesis and Characterization of CuAlO2 and AgAlO2 Delafossite Oxides through Low-Temperature Hydrothermal Methods. *Inorg. Chem.* **2014**, *53*, 4106−4116.

(18) Xiong, D.; Xu, Z.; Zeng, X.; Zhang, W.; Chen, W.; Xu, X.; Wang, M.; Cheng, Y.-B. Hydrothermal Synthesis of Ultrasmall CuCrO2 Nanocrystal Alternatives to NiO Nanoparticles in Efficient P-Type Dye-Sensitized Solar Cells. *J. Mater. Chem.* **2012**, *22*, 24760−24768.

(19) Hoffmann, M. M.; Darab, J. G.; Fulton, J. L. An Infrared and X-Ray Absorption Study of the Structure and Equilibrium of Chromate, Bichromate, and Dichromate in High-Temperature Aqueous Solutions. *J. Phys. Chem. A* **2001**, *105*, 6876−6885.

(20) Creissen, C. E.; Warnan, J.; Antón-García, D.; Farré, Y.; Odobel, F.; Reisner, E. Inverse Opal CuCrO2 Photocathodes for H2 Production Using Organic Dyes and a Molecular Ni Catalyst. *ACS Catal.* **2019**, *9*, 9530−9538.

(21) Ketir, W.; Saadi, S.; Trari, M. Physical and Photoelectrochemical Characterization of CuCrO2 Single Crystal. *J. Solid State Electrochem.* **2012**, *16*, 213−218.

(22) Beverskog, B.; Puigdomenech, I. Revised Pourbaix Diagrams for Copper at 25 to 300°C. *J. Electrochem. Soc.* **1997**, *144*, 3476−3483.

(23) Beverskog, B.; Puigdomenech, I. Revised Pourbaix Diagrams for Chromium at 25−300 °C. *Corros. Sci.* **1997**, *39*, 43−57.

(24) Sanchez-Hachair, A.; Hofmann, A. Hexavalent Chromium Quantification in Solution: Comparing Direct UV−Visible Spectrometry with 1,5-Diphenylcarbazide Colorimetry. *C. R. Chim.* **2018**, *21*, 890−896.

(25) Leita, L.; Margon, A.; Pastrello, A.; Arčon, I.; Contin, M.; Mosetti, D. Soil Humic Acids May Favour the Persistence of Hexavalent Chromium in Soil. *Environ. Pollut.* **2009**, *157*, 1862−1866.

(26) Kerridge, D. H.; Mosley, M. Molten Potassium Thiocyanate: Reactions with Compounds of Chromium. *J. Chem. Soc. Inorg. Phys. Theor.* **1967**, 1874−1879.

(27) Liu, H.; Zhu, W.; Ding, X.; Huang, Y.; Bo, M. Abnormal Deviation of Temperature−Resistivity Correlation for Nanostructured Delafossite CuCrO2 Due to Local Reconfiguration. *J. Phys. Chem. C* **2020**, *124*, 28555−28561.

(28) Jiang, T.; Li, X.; Bujoli-Doeuff, M.; Gautron, E.; Cario, L.; Jobic, S.; Gautier, R. Modulation of Defects in Semiconductors by Facile and Controllable Reduction: The Case of p-Type $CuCrO_2$ Nanoparticles. *Inorg. Chem.* **2016**, *55*, 7729−7733.

(29) Bredar, A. R. C.; Blanchet, M. D.; Comes, R. B.; Farnum, B. H. Evidence and Influence of Copper Vacancies in P-Type $CuGaO_2$ Mesoporous Films. *ACS Appl. Energy Mater.* **2019**, *2*, 19−28.

(30) Yu, M.; Draskovic, T. I.; Wu, Y. Understanding the Crystallization Mechanism of Delafossite CuGaO2 for Controlled Hydrothermal Synthesis of Nanoparticles and Nanoplates. *Inorg. Chem.* **2014**, *53*, 5845−5851.

(31) Subramaniam, T.; Kesavan, G.; Venkatachalam, G. Development of CuAlO2-Encapsulated Reduced Graphene Oxide Nanocomposites: An Efficient and Selective Electrocatalyst for Detection of Neurodegenerative Disorders. *ACS Appl. Bio Mater.* **2020**, *3*, 7769−7778.

(32) Draskovic, T. I.; Yu, M.; Wu, Y. 2H-$CuScO_2$ Prepared by Low-Temperature Hydrothermal Methods and Post-Annealing Effects on Optical and Photoelectrochemical Properties. *Inorg. Chem.* **2015**, *54*, 5519−5526.

https://doi.org/10.1021/acs.inorgchem.2c00943
Inorg. Chem. XXXX, XXX, XXX−XXX